Ultracold quantum gases in triangular optical lattices

To cite this article: C Becker *et al* 2010 *New J. Phys.* **12** 065025

View the article online for updates and enhancements.

You may also like

Ultracold quantum gases in triangular optical lattices

C Becker[1,3], P Soltan-Panahi[1], J Kronjäger[2], S Dörscher[1], K Bongs[2] and K Sengstock[1]

[1] Institut für Laserphysik, Universität Hamburg, Hamburg D-22761, Germany
[2] MUARC, School of Physics and Astronomy, University of Birmingham, Edgbaston, Birmingham B15 2TT, UK
E-mail: cbecker@physnet.uni-hamburg.de

Abstract. Over recent years, exciting developments in the field of ultracold atoms confined in optical lattices have led to numerous theoretical proposals devoted to the quantum simulation of problems e.g. known from condensed matter physics. Many of those ideas demand experimental environments with non-cubic lattice geometries. In this paper, we report on the implementation of a versatile three-beam lattice allowing for the generation of triangular as well as hexagonal optical lattices. As an important step, the superfluid–Mott insulator (SF–MI) quantum phase transition has been observed and investigated in detail in this lattice geometry for the first time. In addition to this, we study the physics of spinor Bose–Einstein condensates (BEC) in the presence of the triangular optical lattice potential, especially spin changing dynamics across the SF–MI transition. Our results suggest that, below the SF–MI phase transition, a well-established mean-field model describes the observed data when renormalizing the spin-dependent interaction. Interestingly, this opens up new perspectives for a lattice-driven tuning of a spin dynamics resonance occurring through the interplay of the quadratic Zeeman effect and spin-dependent interaction. Finally, we discuss further lattice configurations that can be realized with our setup.

[3] Author to whom any correspondence should be addressed.

Contents

1. Introduction

The physics of quantum degenerate gases in optical lattices has rapidly grown to one of the most accounted fields of atomic physics over the last couple of years [1]. This new experimental environment opens the way to studying many-body physics from the so-called mean-field-dominated physics to strongly correlated regimes and allows for a vast amount of interesting experiments ranging from Josephson junctions [2], quantum registers [3] and ultracold chemistry [4] to the implementation of solid state models [5] and experiments concerning spin oscillations in deep optical lattices [6], to name only a few examples. However, to date, nearly all experiments with ultracold atoms have been performed in simple cubic lattices owing to the fact that their experimental implementation is easy compared with other lattice geometries [7]. It is only recently that experimental and theoretical interest in more complex lattice configurations, such as arrays of fully controllable double wells [8]–[10] or artificially generated gauge potentials [11, 12], has appeared. In particular, it has been proposed [13]–[17] that cold atoms loaded into triangular or hexagonal optical lattices exhibit very rich new phases showing e.g. supersolidity [13, 15], quantum stripe ordered states [16], exotic superconducting states [17] or graphene-like physics [18, 19]. In solid state physics, frustrated quantum magnets on triangular or trimerized lattices attract the greatest amount of interest due to their intrinsic link to high-temperature superconductivity (see e.g. [20] and references therein). Recently, it was proposed how frustrated quantum magnets can be realized within a triangular optical lattice [21].

In the context of magnetic interaction in ultracold quantum gases, spin mixtures are currently receiving rapidly growing experimental and theoretical interest. They combine the unprecedented control achieved in single-component Bose–Einstein condensates (BEC) with intrinsic degrees of freedom. The spin-dependent coupling connects quantum gas physics to fundamental magnetic phenomena. Earlier work analyzed the ground states and dynamical evolution of ^{23}Na [22, 23] and ^{87}Rb [24]–[30] spinor condensates in various ground state hyperfine manifolds. Fascinating phenomena, like spontaneous symmetry breaking [31], dynamical instabilities leading to pattern formation [32, 33] as well as dipolar effects [34], have

been observed in harmonically trapped spinor condensates. However, experiments dedicated to the investigation of multicomponent systems in optical lattices have been restricted to isolated two- and three-body spin changing oscillations deep in the Mott-insulating regime [6, 35]. The oscillations observed by these authors could be described within a Rabi-like model, which is different from the mean-field-driven dynamical evolution in harmonically trapped BEC. The physics of spinor condensates in the presence of periodic potentials but still in the superfluid regime is so far widely unexplored.

In this paper, we report on a new experimental setup realizing an ^{87}Rb BEC in a triangular optical lattice [7]. We focus on a concise understanding of the Mott-insulator (MI) transition in the triangular lattice, which is a necessary precondition for further experiments on quantum magnetism in weakly as well as strongly correlated regimes. In particular, we work on a two-dimensional (2D) system, where the higher-dimensional degrees of freedom are frozen out by a sufficiently tight transverse confinement mediated by a 1D lattice.

Furthermore, we investigate the spin dynamics of ^{87}Rb $F = 1$ spinor BEC in this new lattice geometry.

## 2. The three-beam lattice

We start with a description of the experimental realization of the triangular optical lattice. The periodic potential employed in our experiment is created by three laser beams that intersect in the x–y plane mutually enclosing angles of $120°$ with lattice vectors $\mathbf{k}_1 = k\,(0, 1)$, $\mathbf{k}_2 = k\,(-\sqrt{3}/2, -1/2)$ and $\mathbf{k}_3 = k\,(\sqrt{3}/2, -1/2)$ (figure 1(a)). k is the wave vector of the laser employed for the lattice beams. Adding up the field strengths of the individual beams coherently

$$\mathbf{E}_{2D}(\mathbf{r}, t) = \sum_{i=1}^{3} E_{0\,i}\ \varepsilon_i \cos(\mathbf{k}_i \mathbf{r} - \omega t + \phi_i) \tag{1}$$

and averaging over time result in a potential that can be written as

$$V(\mathbf{r}) = V_0 \left(\tfrac{3}{4} + \tfrac{1}{2} \left(\cos(\mathbf{b}_1 \mathbf{r}) + \cos(\mathbf{b}_2 \mathbf{r} + \phi_{12}) + \cos((\mathbf{b}_1 - \mathbf{b}_2)\mathbf{r} + \phi_{23}) \right) \right) \tag{2}$$

for the case that all ε_is are the same, i.e. the polarization is perpendicular to the plane spanned by the lattice beams. The relative phases ϕ_{ij} are stabilized in the experiment to a constant value, which will be set to zero in the following without loss of generality. $V_0 = 4I_0$ corresponds to the depth of a 1D lattice created by two counterpropagating beams, where I_0 is the light shift produced by one of the lattice beams. The corresponding reciprocal lattice vectors $\mathbf{b}_i$ can simply be derived through the relation $\mathbf{b}_i = \epsilon_{ijk}(\mathbf{k}_j - \mathbf{k}_k)$, while the primitive direct lattice vectors follow according to $\mathbf{a}_i \cdot \mathbf{b}_j = 2\pi\,\delta_{i,j}$. The resulting potential is plotted in figure 1(a) and obeys a triangular symmetry. It is important to note that in this configuration the polarization is purely linear and the potential therefore almost m_F-independent for large laser detuning. Note that a variation of the phases ϕ_i of the laser beams only affects the lattice through a global shift in position. Since the ϕ_is can be readily controlled, this very fact can be employed to move, accelerate or even rotate the lattice [21]. So far unexplored lattices characterized by e.g. anisotropic tunneling or a change of sign in the tunneling matrix element J can be created in this way. However, the investigation of these systems is beyond the scope of this publication and will be presented elsewhere. In order to directly illustrate the effect of the triangular lattice structure at this point, figure 2(a)

(a)

(b)
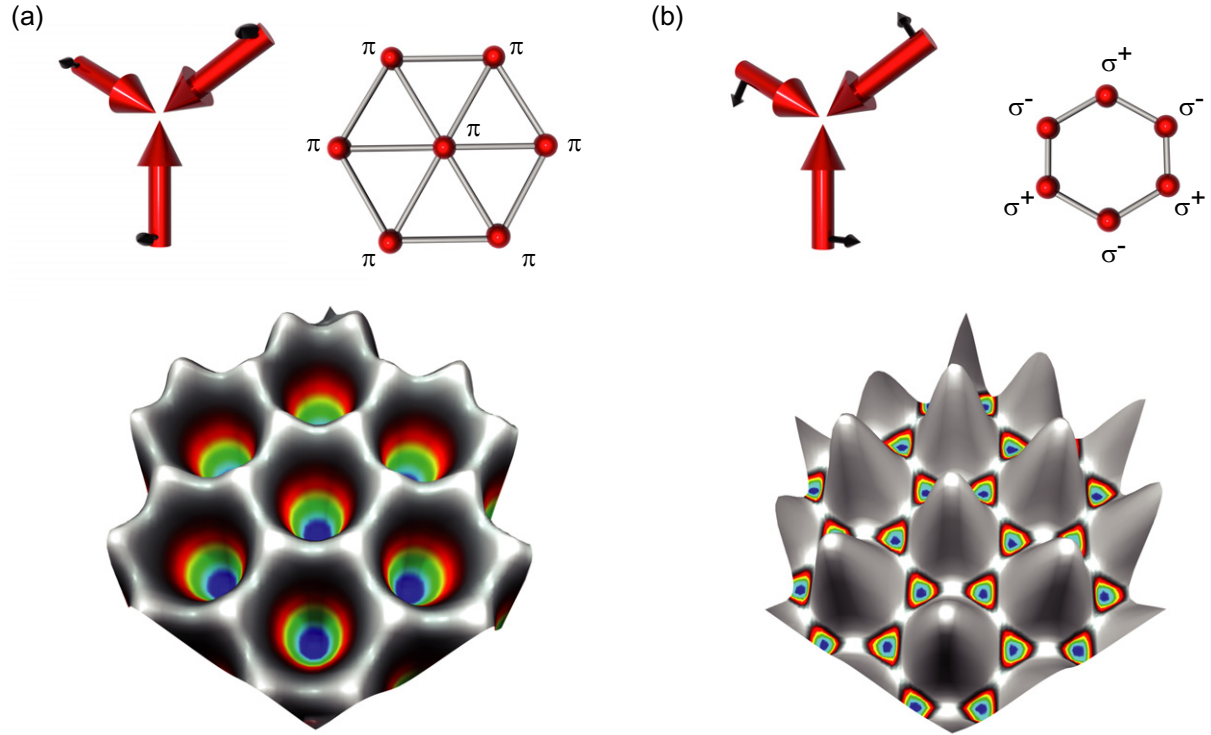
Figure 1. Three beams intersecting in a plane and enclosing angles of 120° pairwise create a triangular optical lattice if their polarization is perpendicular to the plane (a). When the polarization is rotated into the plane spanned by the lattice beams (b), a hexagonal lattice with alternating circular polarization at the potential minima is obtained. A perpendicular 1D lattice provides an overall 3D periodic confinement.

shows absorption images that have been obtained after switching off all optical potentials abruptly, which projects the quasi-momentum distribution in the lattice on free momentum states. Neglecting interaction effects, the density distribution after a sufficiently long time-of-flight (TOF) therefore represents the quasi-momentum distribution in the lattice [36], which directly reveals the reciprocal lattice of the triangular lattice shown in figure 2(a). Opposed to that, figure 2(b) reveals the shape of the first Brillouin zone that can be obtained by first populating the whole first band by carefully exciting the atoms followed by an adiabatic ramp-down of the lattice potential, thereby mapping the quasi-momentum on free momentum states.

By rotating the polarization of the three lattice beams in the $x-y$ plane, as depicted in figure 1(b), another lattice geometry can be realized. The potential minima are now ordered on a hexagonal lattice, as shown in figure 1(b). Moreover, the polarization at the potential minima is perfectly circular and alternating in helicity for nearest-neighboring sites. For alkali atoms, such as ^{87}Rb, the dipole force can be rewritten in a very instructive form if the laser detuning Δ is of the order of the fine-structure splitting Δ_{FS} in ^{87}Rb

$$U_{\mathrm{dip}}(\mathbf{r}) = \frac{3\pi c^2}{2\omega_0^3} \frac{\Gamma}{\Delta} \left(1 + \frac{1}{3}\mathcal{P}(\mathbf{r}) g_F m_F \frac{\Delta_{FS}}{\Delta} \right) I(\mathbf{r}), \tag{3}$$

(a)

(b)
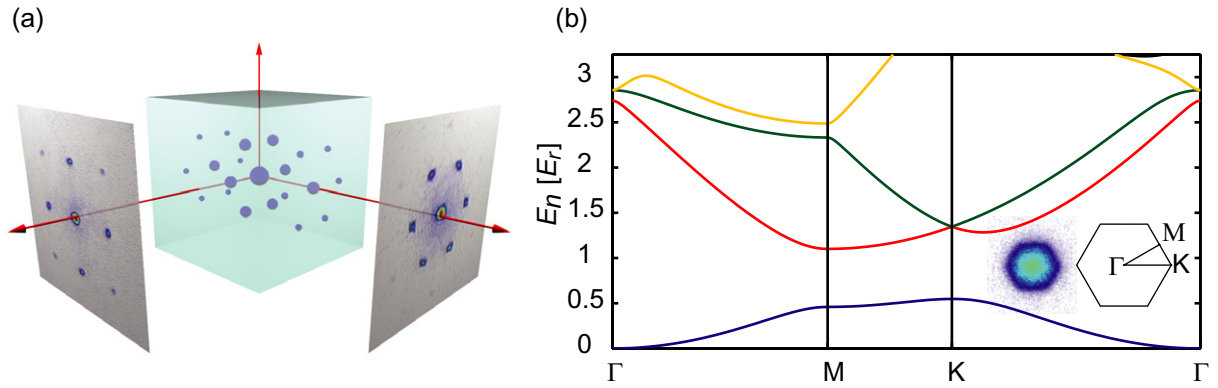
Figure 2. (a) Absorption images of ultracold atoms released from a triangular optical lattice. The sample has been imaged from two different directions. (b) Result of a full 2D band structure calculation for the triangular optical lattice for a lattice depth of $3\,E_{\mathrm{R}}$. The lowest four bands are presented along lines connecting points of high symmetry, as depicted in the inset. An experimental TOF image of the Brillouin zone is also shown.

where ω_0 is the laser frequency, m_F is the magnetic sub-state of the atoms and $\mathcal{P}(\mathbf{r})$ characterizes the spatially varying laser polarization ranging from -1 to $+1$, i.e. either a fully σ^-- or a fully σ^+-polarized laser field. This gives a clear indication that for circular polarization the dipole potential will obey a spin dependence, which vanishes asymptotically for infinite detuning. Taking this into account, the hexagonal lattice will induce an anti-ferromagnetic ordering for atoms with $m_F \neq 0$. As a consequence, atoms with opposite sign in their respective m_F numbers will eventually be trapped at different sites within the lattice. To obtain a quantitative expression for the hexagonal potential, it is convenient to decompose the electric field into its components in a circular basis $\mathbf{e}_{\sigma\pm}$. The corresponding potential for the two polarizations is thus given by

$$V_+ = \frac{V_0}{8}\left(3 + 2(\cos(\mathbf{b}_1 \cdot \mathbf{r} - 2\phi_c) - \cos(\mathbf{b}_2 \cdot \mathbf{r} - \phi_c) + \cos((\mathbf{b}_1 - \mathbf{b}_2)\cdot\mathbf{r} - 2\phi_c)\right), \tag{4}$$

$$V_- = \frac{V_0}{8}\left(3 + 2(-\cos(\mathbf{b}_1 \cdot \mathbf{r} - \phi_c) + \cos(\mathbf{b}_2 \cdot \mathbf{r} - 2\phi_c) + \cos((\mathbf{b}_1 - \mathbf{b}_2)\cdot\mathbf{r} + 2\phi_c)\right), \tag{5}$$

with the characteristic phase $\phi_c = \pi/3$.

These two expressions clearly emphasize that the translational symmetry of the underlying sub-lattices is exactly the same as for the triangular lattice. The change in polarization only corresponds to a change in the local basis with respect to the position of the individual potential wells inside a primitive cell.

By finding the maxima of the above expressions, one can easily show that the primitive cell of the hexagonal lattice contains an anti-ferromagnetic basis with one σ^+-well at $\mathbf{a}_1^\star = 1/3\,(\mathbf{a}_1 + 2\mathbf{a}_2)$ and one σ^--well at $\mathbf{a}_2^\star = 1/3\,(2\mathbf{a}_1 + \mathbf{a}_2)$. Disregarding the m_F-dependence as justified for $|F, 0\rangle$, the pure intensity modulation given by the sum of the two terms in 5 can be written as

$$V_{2D}^\pm(\mathbf{r}) = V_0 \left(\tfrac{3}{4} - \tfrac{1}{4}\left(\cos(\mathbf{b}_1 \cdot \mathbf{r}) + \cos(\mathbf{b}_2 \cdot \mathbf{r}) + \cos((\mathbf{b}_1 - \mathbf{b}_2)\cdot\mathbf{r})\right)\right). \tag{6}$$

For other m_F-states of ^{87}Rb in $F = 2$ and a laser wavelength of 830 nm, the relative difference in the optical dipole potential can be as large as $(U_{\mathrm{dip}}^{|+2\rangle} - U_{\mathrm{dip}}^{|-2\rangle})/U_{\mathrm{dip}}^{|0\rangle} \approx 20\%$, according to equation (3). We emphasize that the interplay between spin-dependent contact interaction, frustrated inter-site dipolar interaction and a spin-dependent trapping potential where e.g. spin-dependent tunneling could be realized may give rise to a whole range of new physical effects and exotic ground state phases.

3. Experimental preparation of BEC and lattice calibration

In the following, we briefly summarize the experimental sequence employed for the measurements presented here. BEC is produced by first collecting up to 10^{10} ^{87}Rb atoms in a double magneto-optical trap system, and subsequently loading them in a magnetic trap of hybrid D-cloverleaf type. Evaporative cooling leaves us with about 1.5×10^6 ultracold atoms slightly above the critical temperature for BEC. Afterwards, the atoms are transferred to a crossed dipole trap with typical trapping frequencies $\bar{\omega} = 2\pi \times (90 \pm 3)$ Hz. The large detuning of the employed Nd : YAG laser with a wavelength of $\lambda = 1064$ nm ensures spin-state-independent global trapping, allowing for the investigation of spinor physics at all lattice depths. Further evaporative cooling by smoothly lowering the intensity of the dipole trap laser beams produces BEC with particle numbers in the range from 6–7×10^4 without any discernible thermal fraction. Since we are especially interested in the physics induced by the triangular lattice, we eliminate the influence of the third dimension by creating a stack of quasi-2D disc-shaped condensates. This is done by ramping up a 1D lattice over 150 ms to a final depth of $V_0 = 30 E_r$, where the recoil energy is given by $E_r = (\hbar k_{\mathrm{lattice}})/2m_{\mathrm{Rb}}$. After this step the tunneling along the perpendicular direction $\hbar/J_{\mathrm{1D}} \approx 0.5\,\mathrm{s}^{-1}$ is negligible compared with the time needed for the experiment $\tau_{\mathrm{exp}} = 0.17$ s. The condition for being in the so-called quasi-2D regime, which requires $k_B T$, $\mu \ll \hbar\omega_{\mathrm{1D}} = \hbar \cdot 2\pi \cdot 21\,\mathrm{kHz} = k_B \cdot 1\,\mu\mathrm{K}$, is also well fulfilled.

The increased effective coupling (see e.g. [37]) $\tilde{g} = g_0 \int \Psi_\perp(\mathbf{r})\,\mathrm{d}\mathbf{r} \approx 2.5 g_0$ leads to a slight expansion of the condensate in all directions, whereas the enhanced harmonic confinement $\tilde{\omega} = 1.2\bar{\omega}_0$ tends to compress the sample. After all we fill about 40 discs, where the occupation of the central disc amounts to $N_{\mathrm{2D}} \approx 4000$. The chemical potential is $\mu = h \cdot 2.7\,\mathrm{kHz} = 133\,\mathrm{nK}$. Subsequently, the triangular 2D lattice is ramped up to the desired final lattice depth using a smooth sigmoidal ramp within 150 ms [38]. After a short hold time of 5 ms, all optical potentials are switched off within less than 10 μs and the atomic cloud is imaged on a CCD camera after 21 ms TOF.

The lattice laser beams are derived from a frequency- and intensity-stabilized Ti : sapphire laser, which delivers up to 1.3 W of power at a wavelength of 830 nm. Beam shaping telescopes focus the laser beams to Gaussian waists of 125 μm. Special care has to be devoted to the relative phases of the three laser beams generating the triangular lattice. Since optical fibers are used to deliver the optical power to the experiment, fast servo loops eliminating any phase noise imprinted by acoustic Brillouin scattering inside the fibers are employed. The measured residual rms-phase noise of the individual laser beams does not exceed $\sqrt{\langle\phi^2\rangle} < 0.12$. This avoids the heating caused by parametric excitation [7, 39].

We calibrate the lattice depth by parametric excitation [39] from the first to the third band at sufficiently large laser power, where the bandwidth of the bands becomes negligibly small, and by comparison of the observed frequencies with band structure calculations (figure 2(b) shows a full 2D band structure calculation). For this purpose, we create 1D lattices using two of

the three laser beams and permute through all pairs of beams to create a potential as symmetric as possible.

## 4. Observation of the superfluid–Mott insulator (SF–MI) transition

The SF–MI transition of ultracold atoms confined in an optical lattice has been under wide investigation over the last decade since the first pioneering theoretical [40, 41] and experimental [42] studies. Many aspects and characteristic features of this quantum phase transition have been addressed, such as the visibility of interference peaks [36], [43]–[45], the possibility of observing a fine structure in the central peak [46, 47] and probing of the energy gap in the MI phase [42], and as a striking demonstration of strong correlations in the MI phase, noise correlations have been observed in various experiments [48]. Moreover, continuative experiments could directly map the wedding cake-like shell structure of different single-site occupation numbers in the MI by high-resolution tomography [49], high-accuracy radiofrequency (rf)-spectroscopy [50] and direct *in situ* imaging [51]. The effects of finite temperature [52]–[55] and dimensionality [56] have also been the focus of interest. A detailed understanding of the MI state is an indispensable requirement for many fascinating experiments that have been proposed in the field of quantum information processing [57] and simulation of solid state systems [5].

Following the experimental sequence outlined above, we have investigated the SF–MI transition in a triangular optical lattice for the first time. Figure 3(a) shows a series of TOF absorption images obtained by varying the lattice depth across the SF–MI transition. We have checked the reversibility of the ramp process by first bringing the system deep in the MI regime and subsequently ramping the lattice down to a depth corresponding to maximal visibility and holding the atoms for a short time comparable with the tunneling time $J/\hbar$, after which we observe a very high recurrence of the visibility.

4.1. Visibility

The visibility, determined as described in [43] and averaged over 15–20 experimental realizations, is shown in a (semi-logarithmic) plot versus the Hubbard parameter η in figure 3(b). The visibility of the diffraction peaks corresponding to reciprocal lattice vectors starts to smear out at a lattice depth of about 3.5 E_R corresponding to a Hubbard parameter $\eta = U/zJ$ close to the expected critical value of $\eta_c = 5.8$ [58] and drops to very small values for a lattice depth $V_0 \geqslant 8E_r$. Note that the number of nearest neighbors z enters the calculation to determine the critical Hubbard parameter according to the mean-field ansatz promoted in [58]. The values for η_c we have found experimentally are not consistent with any other number than $z = 6$, which is expected for the triangular lattice. In an inhomogeneous system a typical feature of a perfect atomic MI is a wedding cake-like structure of the occupation number per lattice site [41]. The relatively strong inhomogeneity in our experiment resulting from the large trapping frequencies of the dipole trap suggests a rather pronounced structure of alternating MI and superfluid shells [43, 44, 49, 50, 59] with a central site occupation $\hat{n}$ of 3–4 atoms. Consequently, reproducible kinks in the visibility are observed, as also reported in [43]. The locations of the kinks fit well to the critical values of the Hubbard parameter η_c^n for the transition to an MI with occupation number n derived from a mean-field model [58].
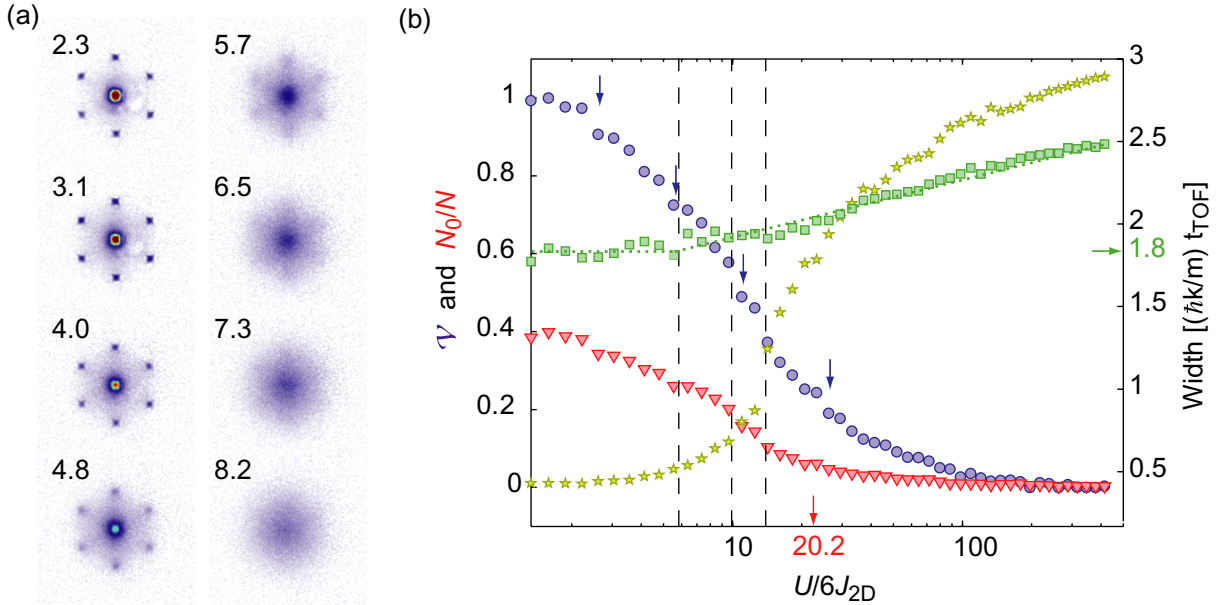
Figure 3. (a) Absorption images of atoms released from a triangular optical lattice for various lattice depths given in units of E_r. (b) Visibility of the interference peaks (blue circles) across the phase transition against U/zJ. Note that the visibility has been normalized to its maximum value of $\mathcal{V}_{max} = 0.48$. The visibility starts to drop around a lattice depth of 3.5–4 E_r. Reproducible kinks marked by blue arrows may indicate the formation of Mott shells. The condensate fraction (red triangles) decreases as the lattice is ramped to deeper values. Pronounced kinks coinciding with those observed for the visibility are observed. The condensate fraction vanishes more quickly than the visibility ($N_0/N = 0$ indicated by red arrow). The FWHM of the central peak of the momentum distribution (yellow stars) is constant for low lattice depth. Around the phase transition it quickly starts to grow—also exhibiting small but reproducible kinks. The width of the incoherent background is plotted for completeness (green squares). Constant below the phase transition where it is a measure for the temperature (indicated by a green arrow), it starts to increase linearly with respect to U/zJ in the MI regime as expected from perturbation theory. The dashed vertical lines indicate the critical values for the transition to an MI state with $\bar{n} = 1, 2$ and 3, respectively.

4.2. Condensate fraction

As the visibility starts to drop, the central as well as the diffraction peaks begin to broaden significantly, as can also be deduced from figure 3(b). We have fitted a bimodal distribution with a fixed condensate width[4] to the peripheral peaks of the interference pattern, as shown in figure 4. In order to account for interaction-induced broadening, data from the first Brillouin zone have been excluded [55, 60]. After sufficiently long TOF, the density distribution consists

---

[4] The condensate width has been determined using fits to data corresponding to low lattice depths well below the phase transition.
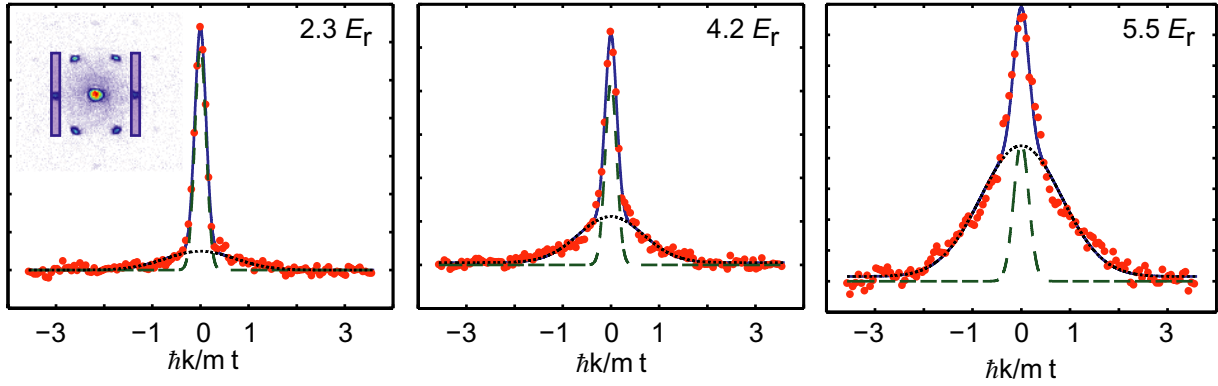
Figure 4. Bimodal fits to the peak structure of the absorption images. Data from the first Brillouin zone have been excluded to minimize interaction effects during the expansion. The data points consequently represent an average of all six satellite peaks (blue shaded area in the inset). Note that every absorption picture has been averaged over 20–30 experimental runs. From left to right, the lattice depth increases, reaching the critical point for singly occupied lattice sites in the last picture.

of sharp interference peaks [36] caused by the condensed atoms, which are assumed to exhibit the same parabolic shape as the external harmonic confinement. The other part of the bimodal density distribution is produced by thermal atoms whose distribution has been modeled employing a Gaussian. For small lattice depths this seems reasonable for a bimodal BEC in a harmonic trap *perturbed* by a periodic potential. For deep lattices the envelope of the density distribution is given by the Fourier transform of the Wannier function $|w(\mathbf{q})|^2$, which is again well approximated by a Gaussian. The condensate fraction determined in this way is also plotted and accurately follows the decrease of visibility in shape for shallow to intermediate lattices. This is as expected since the contrast of the interference pattern is intrinsically connected to the superfluid density [61].

4.3. Residual visibility—particle–hole excitations

For lattice depths close to the expected SF–MI phase transition, the superfluid fraction disappears while a small residual visibility persists, even far in the MI regime. This residual visibility in the MI regime has been attributed to excitations in terms of particle–hole pairs [43, 44], which should in principle be present at any finite hopping J. We have determined the coefficients α by fitting the model density derived from a first-order perturbed MI state [43, 62] according to $\langle \hat{n}_{\mathbf{k}} \rangle = N |w(\mathbf{k})|^2 (1 + \sum_i \alpha \cos(\pi \mathbf{k}/\mathbf{k}_i))$. The expected value $\alpha = 4J/U\hat{n}(\hat{n}+1)$ fits surprisingly well the observed data for an average occupation number of $\hat{n} = 2$, in spite of the rich shell structure that is expected in our experiment with occupation numbers ranging from 1 to 4 (see figure 5). The error of the applied fit starts to increase significantly (indicated by the intersection of the two red lines in figure 5(b)) at a lattice depth corresponding to the appearance of a finite superfluid fraction, supporting the idea of particle–hole pairs as the origin of the residual visibility.
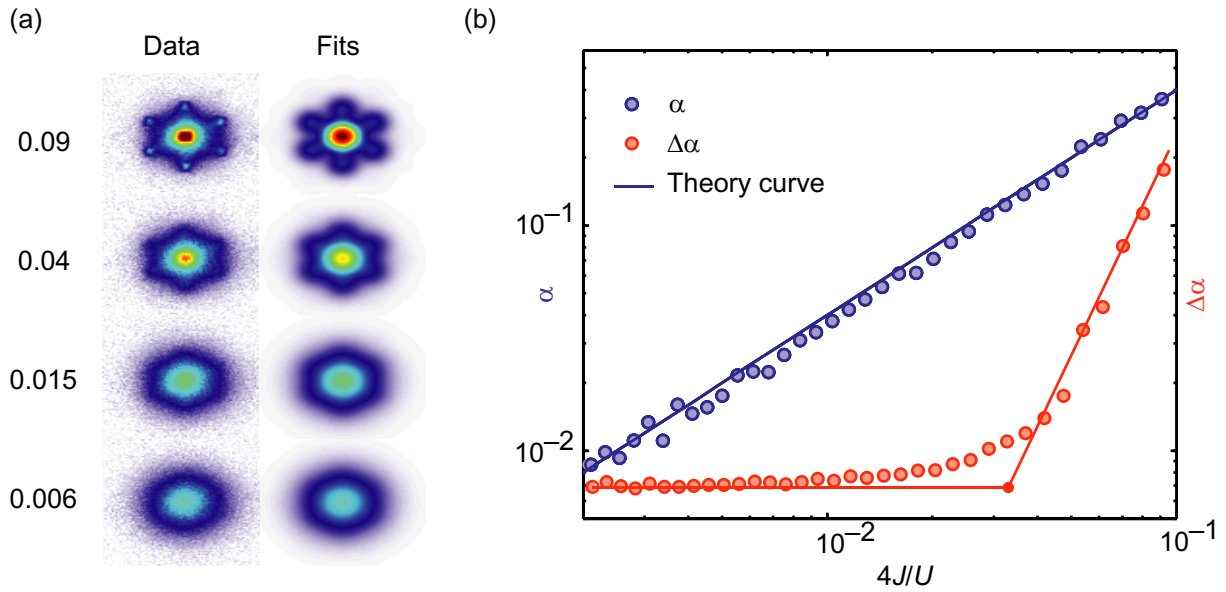
Figure 5. (a) Absorption images of ultracold atoms released from a triangular optical lattice for selected lattice depths above the MI transition point are shown together with fits of first order perturbation theory with only one free parameter α. (b) Experimentally obtained values for α together with the theoretical expected curve for an average occupation of $\langle \hat{n} \rangle = 2$. Note that α is proportional to $8J/U$. The fit error $\Delta\alpha$ exhibits a distinct increase at a Hubbard parameter corresponding to the appearance of a finite superfluid fraction, as indicated by the red arrow in figure 3. The red solid lines are a guide to the eye.

Although recent simulations [54] show that ultracold thermal atoms also exhibit a significant interference pattern, our experimental parameters suggest that loading the atoms into intermediate deep lattices should even result in adiabatic cooling [63]. However, the vanishing of the interference pattern has to be evaluated with great care for atomic samples with a non-negligible thermal fraction (see [36], [63]–[65]). By ramping back from a deep MI state to zero lattice depth and analysis of the density distribution after TOF, we have checked that only negligible heating occurred for short to intermediate hold times.

Note that the broadening of the diffraction peaks as well as the condensate fraction also show a kink-like behavior, supporting the observation derived from the visibility measurement [47].

5. Spin dynamics in a triangular lattice

We have performed measurements of spin dynamics in lattices of different depth and at different magnetic fields in order to gain insight into the physics of magnetic systems in periodic potentials. In principle, one would expect a crossover from mean-field regime spin dynamics as described in e.g. [26] to few-particle spin oscillations isolated at individual lattice sites [6]. It has been found for the latter case that coherent oscillations between two two-particle states $\psi_i = |m_F = 0, 0\rangle \leftrightarrow \psi_f = |-1, 1\rangle$ occur that can be readily explained within the framework of

IOP Institute of Physics ΦDEUTSCHE PHYSIKALISCHE GESELLSCHAFT

a Rabi-like model [6]. For atoms with $F = 1$ in an optical lattice, the effective Rabi frequency is composed of a coupling strength $\Omega_{\text{if}} \propto g_1 \int |w(\mathbf{r})|^4 \, d\mathbf{r}$ given by the spin-dependent interaction between the two states and a detuning $\delta = \delta_0 + \delta(B^2)$. δ is given by a part proportional to the quadratic Zeeman shift $\delta(B^2)$ and an offset term determined by the difference in interaction energy of the initial and final states $\delta_0 \propto g_1/2$.

Here we focus on the investigation of spin dynamics at intermediate lattice depths, which is associated with an overall spin *independent* trapping potential from the beginning. We present measurements of spin dynamics of ^{87}Rb BEC in $F = 1$, starting in an almost isotropic crossed optical dipole trap and ranging across the superfluid regime and up to the SF–MI phase transition inside a triangular optical lattice. In addition, the magnetic field has been varied in order to change the relative influence of quadratic Zeeman effect and spin-dependent interaction. We show that this ratio determines the behavior of oscillation amplitude and period. After briefly recalling the physics and notations of mean-field spinor physics within the single-mode approximation (SMA) and providing a description of the experimental sequence, we will present results suggesting a new and elegant method to tune the spin dynamics resonance known from experiments in harmonic traps (see e.g. [26, 29]).

5.1. Mean-field theory of spin dynamics

The description of spinor condensates presented here is based on the evolution due to the corresponding mean-field Hamiltonian using the SMA as outlined in more detail in e.g. [26, 27]. Spin mixing occurs as a consequence of two-particle collisions and can be classified by the total spin f of the colliding pair. For $F = 1$ spinor condensates the allowed values are $f = 0$ and 2. The spin mixing interaction can be parameterized by the coupling coefficient $g_1 = (4\pi\hbar^2/m)(a_2 - a_0/3)$, each total spin channel being associated with an s-wave scattering length a_f. The dynamics of the $2F + 1$ components of the vectorial spinor order parameter directly follows from the resulting mean-field energy functional for the spin part of the wave function ζ:

$$\langle H_{\text{spin}} \rangle = \frac{\hbar}{2} N \langle n \rangle (g_1 \langle \mathbf{F} \rangle^2) + \hbar N(-p\langle F_z \rangle + q\langle F_z^2 \rangle) \tag{7}$$

with

$$\langle F_z \rangle \equiv \sum_{ij} \zeta_i^* (F_z)_{ij} \zeta_j, \tag{8}$$

$$\langle F_z^2 \rangle \equiv \sum_{ijk} \zeta_i^* (F_z)_{ik} (F_z)_{kj} \zeta_j. \tag{9}$$

$|p| = \frac{1}{2}(\mu_B/\hbar)B_0$ and $|q| = p^2/\omega_{\text{hfs}}$ parameterize the linear and quadratic Zeeman effects, respectively. The dynamics governed by the above Hamiltonian can be solved exactly for $F = 1$ and a particular initial state $\zeta_{\pi/2}$ that can be easily prepared experimentally by the application of an initial $\pi/2$ rf pulse [26, 27]. The solution of the resulting equation of motion for the populations of the individual m_F-states can be expressed in terms of Jacobi elliptical functions (JEF)

$$|\zeta_0(t)|^2 = (1 - k \, \text{sn}_k^2(qt))/2, \tag{10}$$

$$|\zeta_{\pm 1}(t)|^2 = (1 + k \, \text{sn}_k^2(qt))/4. \tag{11}$$

The occurrence of the parameter $k = g_1 \langle n \rangle / q$ in the analytic solution indicates that the amplitude and oscillation period of spin dynamics are determined by the ratio of interaction to quadratic Zeeman energy. The JEF in equation (11) can be further simplified by approximations in two limiting cases:

5.1.1. Zeeman regime ($k \ll 1$). In the Zeeman regime, where the quadratic Zeeman effect dominates over spin-dependent interaction, the JEF can be approximated by ordinary trigonometric functions $\mathrm{sn}_k(x) \approx \sin(x)$ and $\mathrm{cn}_k(x) \approx \cos(x)$, $\mathrm{dn}_k(x) \approx 1$, yielding

$$|\zeta_0(t)|^2 \overset{\mathrm{ZMR}}{=} (1 - k \, \sin^2(qt))/2. \tag{12}$$

The amplitude of the oscillation is proportional to k, while the period is simply given by π/q.

5.1.2. Interaction regime ($k \gg 1$). In this regime, the spin-dependent interaction dominates any dynamics. The appropriate approximations for the JEF read $\mathrm{sn}_k(x) = 1/k \, \sin_{1/k}(kx)$, resulting in population oscillations

$$|\zeta_0(t)|^2 \overset{\mathrm{IAR}}{=} (1 - 1/k \, \sin^2(g_1 \langle n \rangle t))/2. \tag{13}$$

Now the amplitude scales as $1/k$ and the spin-dependent interaction determines the period $\pi/g_1 \langle n \rangle$.

In the intermediate regime where both energies are of the same order of magnitude, a spin dynamics resonance will occur, which was observed for the first time in a harmonically trapped ^{87}Rb $F = 2$ spinor condensate in [27].[5]

Note that the tuning of the resonance in the aforementioned experiments [27] has been achieved by changing the magnetic field value while keeping the atomic density as constant as possible.

5.2. Spin dynamics of ^{87}Rb $F = 1$ spinor condensates in a triangular lattice

In this paper, we discuss for the first time that the mean-field spin dynamics resonance persists even in the presence of a periodic potential, as long as a significant superfluid fraction is still present in the system. Moreover, the renormalization of the spin-dependent interaction by the lattice potential allows for an effective tuning of the resonance at constant magnetic field.

The experimental procedure for the results presented here is as follows. After preparation of BEC in $|1, -1\rangle$ with particle numbers of $N \approx 10^5$ and no discernible thermal fraction, we load the atoms in the 3D optical lattice consisting of a 2D triangular lattice and a perpendicular 1D standing wave, as discussed above. For these measurements, the individual lattice depths have been adapted to yield equal U/zJ for the different spatial directions. After the final lattice depth has been reached, we allow the system to relax to equilibrium for 5 ms before we apply a $\pi/2$-pulse to prepare the initial state $\zeta_{\pi/2}$. The magnetic field is then abruptly switched to the desired final value. We then hold the atoms for a variable evolution time to allow spin dynamics to take place. In order to have atomic samples that are *not* optically thick after TOF, we quickly ramp

---

[5] $F = 2$ spinor condensates have an additional spin-dependent interaction parameterized by $g_2 \cdot |S_0|^2$. However, due to the smallness of this contribution, the resulting dynamics can well be approximated by the solutions found for $F = 1$.

IOP Institute of Physics ⚫ DEUTSCHE PHYSIKALISCHE GESELLSCHAFT

down the lattice within 5 ms following the end of the evolution time to obtain atomic clouds that allow for a reliable and unambiguous atom number determination. Finally, all trapping potentials are switched off, and after 21 ms of TOF, including Stern–Gerlach separation, the atoms are imaged with resonant light.

In the superfluid regime the addition of a periodic potential should mainly show up in terms of an increased effective spin-dependent coupling owing to an increased mean density of the sample. We expect that the resulting effective k will determine frequency and amplitude of spin dynamics within this model. However, different additional effects, e.g. caused by reduced mobility or an increased thermalization rate, might lead to deviations from this behavior and the data have been carefully analyzed to see whether any indications of those deviations can be found.

To estimate atomic densities in the different lattice regimes, we have employed a Thomas–Fermi-like approximation of the Bose–Hubbard model for the superfluid regime and the regime close to the SF–MI phase transition. The corresponding densities are calculated by taking into account the particular overall harmonic trapping frequencies $\bar{\omega}$, onsite interaction matrix elements U and total particle numbers N according to $\bar{n} = 4/7 \, n_0 = \mu/g_0$ with

$$\mu = \left(\frac{15}{16} \frac{V_{\text{cell}} m^{3/2} N U \bar{\omega}^3}{\sqrt{2}\pi} \right)^{2/5}, \tag{14}$$

where V_{cell} is the volume of a unit cell of the lattice. Having obtained the mean density in this way, a specific effective k value can be assigned to each set of measurements. It should be mentioned that our experimental parameters allow for a tuning of the effective density by a factor of approximately 5 by changing the lattice depth.

Figure 6(a) shows spin dynamics measurements in a crossed dipole trap (Hubbard parameter $\eta = 0$), in the superfluid regime ($\eta = 1.45$) and in the vicinity of the SF–MI phase transition ($\eta = 8.9$) for exemplary magnetic fields. It can be inferred from the graphs that the population in the $m_F = 0$ component ρ_{00} undergoes periodic oscillations. The dynamics of the other components follow according to $\rho_{-1-1} = \rho_{11} = 1/2 \, (1 - \rho_{00})$. Oscillation amplitude and period clearly change, depending on the lattice depth and the magnetic field. The time evolution of the $m_F = 0$ population has been fitted with a function $\rho_{00} = (1 - A \sin^2(B \cdot (t + C)))/2$ to extract the oscillation amplitude A and period $2\pi/B$.

A direct comparison of amplitudes and periods obtained in this way to the analytical mean-field solution equation (11) shows indeed good agreement if the spin-dependent interaction energy entering $k = g_1 \langle n \rangle / q$ is renormalized by the effective density in the optical lattice, as explained above (figure 6(b)). A major consequence of this observation is that, by raising an optical lattice potential, the atomic density and thereby the effective k can be varied, which can readily be used to precisely tune the spin dynamics resonance at constant magnetic field and constant particle number. Beyond that, we want to emphasize that the physics of spinor condensates in optical lattices demands further investigation. For example, the first indication of spin demixing at very low magnetic fields, as well as its suppression with increasing lattice depth, has been observed in our experiments. This effect leads to a slowdown and potentially stop of spin mixing dynamics. The accurate and detailed analysis of this and similar effects is, however, beyond the scope of this paper and will be presented elsewhere.
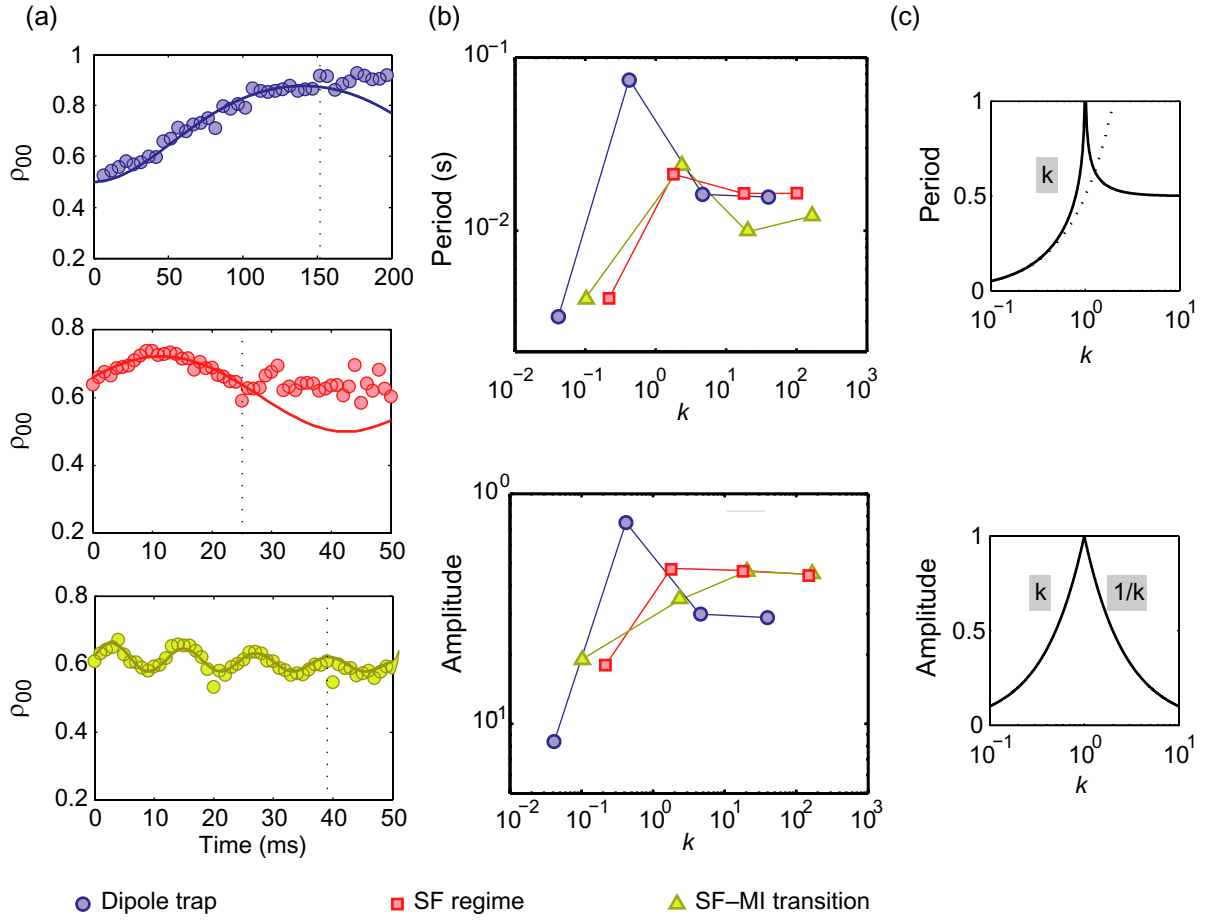
Figure 6. (a) Exemplary measurements of spin mixing dynamics for different strengths of the periodic potential and different magnetic fields. From top to bottom, measurements have been performed in the dipole trap at $|B| = 270\,\text{mG}$, in the superfluid regime at $|B| = 30\,\text{mG}$ and close to the phase transition from superfluid to MI at $|B| = 800\,\text{mG}$. The individual graphs show the time evolution of the population in the $m_F = 0$ state ρ_{00}. Data are presented along with fits (solid lines) to determine the oscillation amplitude and period. (b) Period of spin mixing dynamics as a function of the dimensionless parameter $k_{\text{eff}} = g_1 \langle n_{\text{eff}} \rangle / q$ for experiments in a crossed dipole trap (blue circles), in the superfluid regime in the presence of a triangular optical lattice (red triangles) and close to the quantum phase transition from superfluid to MI (yellow stars). Solid lines are a guide to the eye. (c) Theoretically expected period and amplitude according to equation (11).

6. Conclusion and outlook

In conclusion, we have presented first experiments with ultracold atoms loaded in a triangular optical lattice. In particular, the MI transition has been investigated in a 2D system. In direct comparison to a cubic lattice, the transition occurs at much lower lattice depths due to the much stronger localization of the atoms. Moreover, we have observed spin dynamics of $^{87}\text{Rb}\,F = 1$ spinor condensates in an optical lattice and found qualitative agreement with the mean-field

IOP Institute of Physics ⬤ DEUTSCHE PHYSIKALISCHE GESELLSCHAFT

solution raised in [26] as long as the lattice is shallow enough to maintain a significant superfluid fraction. The differences in the results at different lattice depths can mainly be reduced to an effective spin-dependent interaction $g_1 \langle n_{\mathrm{norm}} \rangle$, which allows for a tuning of the spin dynamics resonance.

Future perspectives include loading and investigation of spinor-BEC in the hexagonal anti-ferromagnetic lattice and analysis of magnetic ground states. Fascinatingly, the sign of the tunneling matrix element J can be reversed by slightly modulating the frequencies of the three laser beams, creating the triangular lattice, as described in [21]. Thereby investigating fascinating model systems known from solid state physics that give rise to effects like Néel ordering and spin liquid phases is made possible. Experiments concerning transport and spin-dependent tunneling for the creation of highly entangled multi-particle states are highly interesting research directions.

Acknowledgments

References

[1] Bloch I, Dalibard J and Zwerger W 2008 Many-body physics with ultracold gases *Rev. Mod. Phys.* **80** 885
[2] Albiez M, Gati R, Fölling J, Hunsmann S, Cristiani M and Oberthaler M K 2005 Direct observation of tunneling and nonlinear self-trapping in a single bosonic–Josephson junction *Phys. Rev. Lett.* **95** 010402
[3] Sorensen A, Duan L-M, Cirac J I and Zoller P 2001 Many-particle entanglement with Bose–Einstein condensates *Nature* **409** 63
[4] Ospelkaus C, Ospelkaus S, Humbert L, Ernst P, Sengstock K and Bongs K 2006 Ultracold heteronuclear molecules in a 3D optical lattice *Phys. Rev. Lett.* **97** 120402
[5] Lewenstein M, Sanpera A, Ahufinger V, Damski B, Sen A and Sen U 2007 Ultracold atomic gases in optical lattices: mimicking condensed matter physics and beyond *Adv. Phys.* **56** 243–379
[6] Widera A, Gerbier F, Fölling S, Gericke T, Mandel O and Bloch I 2005 Coherent collisional spin dynamics in optical lattices *Phys. Rev. Lett.* **95** 190405
[7] Petsas K I, Coates A B and Grynberg G 1994 Crystallography of optical lattices *Phys. Rev.* A **50** 5173
[8] Trotzky S, Cheinet P, Fölling S, Feld M, Schnorrberger U, Rey A M, Polkonikov A, Demler E A, Lukin M D and Bloch I 2008 Time-resolved observation and control of superexchange interaction with ultracold atoms in optical lattices *Science* **319** 295
[9] Cheinet P, Trotzky S, Feld M, Schnorrberger U, Moreno-Cardoner M, Fölling S and Bloch I 2008 Counting atoms using interaction blockade in an optical lattice *Phys. Rev. Lett.* **101** 090404
[10] Anderlini M, Lee P J, Brown B L, Sebby-Strabley J, Phillips W D and Porto J V 2007 Controlled exchange interaction between pairs of neutral atoms in an optical lattice *Nature* **448** 452–6
[11] Lim L K, Smith C M and Hemmerich A 2008 Staggered-vortex superfluid of ultracold bosons in a 3D optical lattice *Phys. Rev. Lett.* **100** 130402
[12] Lin Y-J, Compton R L, Perry A R, Phillips W D, Porto J V and Spielman I B 2009 Bose–Einstein condensate in a uniform light-induced vector potential *Phys. Rev. Lett.* **102** 130401
[13] Melko R G, Paramekanti A, Burkov A A, Vishwanath A, Sheng D N and Barents L 2005 Supersolid order from disorder: hard-core bosons on the triangular lattices *Phys. Rev. Lett.* **95** 127207
[14] Santos L, Baranov M A, Cirac J I, Everts H-U, Fehrmann H and Lewenstein M 2004 Atomic quantum gases in Kagome lattices *Phys. Rev. Lett.* **93** 030601
[15] Wessel S and Troyer M 2005 Supersolid hard-core bosons on the triangular lattice *Phys. Rev. Lett.* **95** 127205

[16] Wu C, Liu W V, Moore J and Sarma S D 2006 Quantum stripe ordering in optical lattices *Phys. Rev. Lett.* **97** 190406

[17] Mathey L, Tsai S-W and Neto A H 2007 Exotic superconducting phases of ulracold atom mixtures on triangular lattices *Phys. Rev.* B **75** 174516

[18] Juzeliunas G, Ruseckas J, Lindberg M, Santos L and Öhberg P 2008 Quasirelativistic behaviour of cold atoms in light fields *Phys. Rev.* A **77** 011802

[19] Haddad L H and Carr L D 2009 The nonlinear Dirac equation in Bose–Einstein condensates: foundation and symmetries *Physica* D **238** 1413–21

[20] Nakatsuji S, Nambu Y, Tonomura H, Sakai O, Jonas S, Broholm C, Tsunetsugu H, Qiu Y and Maeno Y 2005 Spin disorder on a triangular lattice *Science* **309** 1697–700

[21] Eckardt A, Hauke P, Soltan-Panahi P, Becker C, Sengstock K and Lewenstein M 2010 Frustrated quantum antiferromagnetism with ultracold bosons in a triangular lattice *Europhys. Lett.* **89** 10010

[22] Miesner H-J, Stamper-Kurn D M, Stenger J, Inouye S, Chikkatur A P and Ketterle W 1999 Observation of metastable states in spinor Bose–Einstein condensates *Phys. Rev. Lett.* **82** 2228

[23] Stamper-Kurn D M, Miesner H-J, Chikkatur A P, Inouye S, Stenger J and Ketterle W 1999 Quantum tunneling across spin domains in a Bose–Einstein condensate *Phys. Rev. Lett.* **83** 661

[24] Erhard M, Schmaljohann H, Kronjäger J, Bongs K and Sengstock K 2004 Bose–Einstein condensation at constant temperature *Phys. Rev.* A **70** 031602

[25] Schmaljohann H, Erhard M, Kronjäger J, Kottke M, van Staa S, Cacciapuoti L, Arlt J J, Bongs K and Sengstock K 2004 Dynamics of $F = 2$ spinor Bose–Einstein condensates *Phys. Rev. Lett.* **92** 040402

[26] Kronjäger J, Becker C, Brinkmann M, Walser R, Navez P, Bongs K and Sengstock K 2005 Evolution of a spinor condensate: coherent dynamics, dephasing and revivals *Phys. Rev.* A **72** 063619

[27] Kronjäger J, Becker C, Navez P, Bongs K and Sengstock K 2006 Magnetically tuned spin dynamics resonance *Phys. Rev. Lett.* **97** 110404

[28] Chang M-S, Hamleyand C D, Barrett M D, Sauer J A, Fortier K M, Zhang W, You L and Chapman M S 2004 Observation of spinor dynamics in optically trapped ^{87}Rb Bose–Einstein condensates *Phys. Rev. Lett.* **92** 140403

[29] Chang M-S, Qin Q, Zhang W, You L and Chapman M S 2005 Coherent spinor dynamics in a spin-1 Bose condensate *Nat. Phys.* **1** 111

[30] Zhang W, Zhou D L, Chang M-S, Chapman M-S and You L 2005 Coherent spin mixing dynamics in a spin-1 atomic condensate *Phys. Rev.* A **72** 013602

[31] Sadler L E, Higbie J M, Leslie S R, Vengalattore M and Stamper–Kurn D M 2006 Spontaneous symmetry breaking in a quenched ferromagnetic spinor Bose–Einstein condensate *Nature* **443** 312

[32] Kronjäger J, Becker C, Soltan-Panahi P, Bongs K and Sengstock K 2009 Spontaneous pattern formation in an anti-ferromagnetic quantum gas arXiv:0904.2339

[33] Zhang W, Zhou D L, Chang M-S, Chapman M-S and You L 2005 Dynamical instability and domain formation in a spin-1 Bose–Einstein condensate *Phys. Rev. Lett.* **95** 180403

[34] Vengalattore M, Laslie S R, Guzman J and Stamper-Kurn D M 2008 Spontaneously modulated spin textures in a dipolar spinor Bose–Einstein condensate *Phys. Rev. Lett.* **100** 170403

[35] Gerbier F, Widera A, Fölling S, Mandel O and Bloch I 2006 Resonant control of spin dynamics in ultracold quantum gases by microwave dressing *Phys. Rev.* A **73** 041602

[36] Gerbier F *et al* 2008 Expansion of a quantum gas released from an optical lattice *Phys. Rev. Lett.* **101** 155303

[37] Pitaevskii L and Stringari S 2003 *Bose–Einstein Condensation* 1 edn (Oxford: Oxford Science Publications)

[38] Jaksch D, Venturi V, Cirac J I, Williams C J and Zoller P 2002 Creation of a molecular condensate by dynamically melting a Mott insulator *Phys. Rev. Lett.* **89** 040202

[39] Savard T A, O'Hara K M and Thomas J E 1997 Laser-noise-induced heating in far-off resonant optical traps *Phys. Rev.* A **56** R1095–8

[40] Fisher M P A, Weichman P B, Grinstein G and Fisher D S 1989 Boson localization and the superfluid–insulator transition *Phys. Rev.* B **40** 546–70

[41] Jaksch D, Bruder C, Cirac J I, Gardiner C W and Zoller P 1998 Cold bosonic atoms in optical lattices *Phys. Rev. Lett.* **81** 3108–11

[42] Greiner M, Mandel O, Esslinger T, Hänsch T W and Bloch I 2002 Quantum phase transition from a superfluid to a Mott insulator in a gas of ultracold atoms *Nature* **415** 39–44

[43] Gerbier F, Widera A, Fölling S, Mandel O, Gericke T and Bloch I 2005 Phase coherence of an atomic Mott insulator *Phys. Rev. Lett.* **95** 050404

[44] Gerbier F, Widera A, Fölling S, Mandel O, Gericke T and Bloch I 2005 Interference pattern and visibility of a Mott insulator *Phys. Rev.* A **72** 053606

[45] Zwerger W 2003 Mott–Hubbard transition of cold atoms in optical lattices *J. Opt.* B **5** S9–16

[46] Kashurnikov V A, Prokof'ev N V and Svistunov B V 2002 Revealing the superfluid–Mott-insulator transition in an optical lattice *Phys. Rev.* A **66** 031601

[47] Wessels S, Alet F, Troyer M and Batrouni G G 2004 Quantum Monte Carlo simulations of confined bosonic atoms in optical lattices *Phys. Rev.* A **70** 053615

[48] Fölling S, Gerbier F, Widera A, Mandel O, Gericke T and Bloch I 2005 Spatial quantum noise interferometry in expanding ultracold atom clouds *Nature* **434** 481–4

[49] Fölling S, Widera A, Müller T, Gerbier F and Bloch I 2006 Formation of spatial shell structure in the superfluid to Mott insulator transition *Phys. Rev. Lett.* **97** 060403

[50] Campbell G K, Mun J, Boyd M, Medley P, Leonhardt A E, Marcassa L G, Pritchard D E and Ketterle W 2006 Imaging the Mott insulator shells by using atomic clock shifts *Science* **313** 649–52

[51] Gemelke N, Zhang X, Hung C L and Chin C 2009 *In situ* observation of incompressible Mott-insulating domains in ultracold atomic gases *Nature* **460** 995

[52] Gerbier F 2007 Boson Mott insulators at finite temperatures *Phys. Rev. Lett.* **99** 120405

[53] Pupillo G, Williams C J and Prokof'ev N V 2006 Effects of finite temperature on the Mott-insulator state *Phys. Rev.* A **73** 013408

[54] Kato Y, Zhou Q, Kawashima N and Trivedi N 2008 Sharp peaks in the momentum distribution of bosons in optical lattices in the normal state *Nat. Phys.* **4** 617–21

[55] Yi W, Lin G-D and Duan L-M 2007 Signal of Bose–Einstein condensation in an optical lattice at finite temperature *Phys. Rev.* A **76** 031602

[56] Stöferle T, Moritz H, Schori C, Köhl M and Esslinger T 2004 Transition from a strongly interacting 1D superfluid to a Mott insulator *Phys. Rev. Lett.* **92** 130403

[57] Calarco T, Dorner U, Julienne P S, Williams C J and Zoller P 2004 Quantum computations with atoms in optical lattices: marker qubits and molecular interactions *Phys. Rev.* A **70** 012306

[58] van Oosten D, van der Straten P and Stoof H T C 2001 Quantum phases in an optical lattice *Phys. Rev.* A **63** 053601

[59] Mitra K, Williams C J and Sa de Melo C A R 2008 Superfluid and Mott-insulating shells of bosons in harmonically confined optical lattices *Phys. Rev.* A **77** 033607

[60] Spielman I B, Phillips W D and Porto J V 2008 Condensate fraction in a 2D Bose gas measured across the Mott-insulator transition *Phys. Rev. Lett.* **100** 120402

[61] Roth R and Burnett K 2003 Superfluidity and interference pattern of ultracold atoms in optical lattices *Phys. Rev.* A **67** 031602

[62] Spielman I B, Phillips W D and Porto J V 2007 Mott-insulator transition in a two-dimensional atomic Bose gas *Phys. Rev. Lett.* **98** 080404

[63] Blakie P B and Porto J V 2004 Adiabatic loading of bosons into optical lattices *Phys. Rev.* A **69** 013603

[64] DeMarco B, Lannert C, Vishveshwara S and Wei T-C 2005 Structure and stability of Mott-insulator shells of bosons trapped in an optical lattice *Phys. Rev.* A **71** 063601

[65] Ho T-L and Zhou Q 2007 Intrinsic heating and cooling in adiabatic processes for bosons in optical lattices *Phys. Rev. Lett.* **99** 120404